Chem Soc Rev

TUTORIAL REVIEW

View Article Online
View Journal | View Issue

Cite this: *Chem. Soc. Rev.*, 2024, 53, 2284

Chemical multiscale robotics for bacterial biofilm treatment

Carmen C. Mayorga-Martinez,[a] Li Zhang [bc] and Martin Pumera *[adef]

A biofilm constitutes a bacterial community encased in a sticky matrix of extracellular polymeric substances. These intricate microbial communities adhere to various host surfaces such as hard and soft tissues as well as indwelling medical devices. These microbial aggregates form a robust matrix of extracellular polymeric substances (EPSs), leading to the majority of human infections. Such infections tend to exhibit high resistance to treatment, often progressing into chronic states. The matrix of EPS protects bacteria from a hostile environment and prevents the penetration of antibacterial agents. Modern robots at nano, micro, and millimeter scales are highly attractive candidates for biomedical applications due to their diverse functionalities, such as navigating in confined spaces and targeted multitasking. In this tutorial review, we describe key milestones in the strategies developed for the removal and eradication of biofilms using robots of different sizes and shapes. It can be seen that robots at different scales are useful and effective tools for treating bacterial biofilms, thus preventing persistent infections, the loss of costly implanted medical devices, and additional costs associated with hospitalization and therapies.

Received 5th August 2023

DOI: 10.1039/d3cs00564j

rsc.li/chem-soc-rev

Key learning points
(1) Biofilm formation and structure.
(2) Strategies for biofilm treatment using multiscale robots.
(3) Biofilm removal from indwelling medical devices.
(4) *In vivo* and *ex vivo* elimination of biofilms treated using multiscale robots.
(5) Future challenges in biofilm treatment and removal using modern multiscale robots.

1. Introduction

Modern multiscale robots are propelled remotely by external sources such as magnetic, light, and ultrasound fields as well as by the catalysis of chemical fuels.[1–5] Such robots have attracted widespread attention in medical applications due to their impressive abilities to navigate in confined spaces, deliver cargo to targeted places, and perform biosensing and microorganism manipulation.[6–10] Moreover, multiscale robots are composed of several smart materials for their actuation or for performing specific tasks; in many cases, these materials are biocompatible, biodegradable, and scalable.[11–16] Depending on their propulsion mechanism, these robots can be maneuvered with complete control over their direction. Finally, they can swarm and reconfigure their forms to ensure the accomplishment of tasks that a single robot might not be able to achieve.[17–23]

Recently, due to the broad functionality of robots at different scales, they have been used for the removal of different bacterial biofilms. This paper aims to summarize all the achievements made by multiscale robots in the treatment of bacterial biofilms (Fig. 1). First, we will describe the formation and structure of a biofilm and then proceed to the different types of robots used for its removal. For a better understanding, we categorize the robots according to their

[a] *Advanced Nanorobots & Multicale Robotics, Faculty of Electrical Engineering and Computer Science, VSB – Technical University of Ostrava, 17. listopadu 2172/15, Ostrava 70800, Czech Republic. E-mail: martin.pumera@vsb.cz*
[b] *Department of Mechanical and Automation Engineering, The Chinese University of Hong Kong, Hong Kong 999077, China*
[c] *Department of Surgery, The Chinese University of Hong Kong, Hong Kong 999077, China*
[d] *Department of Medical Research, China Medical University Hospital, China Medical University, No. 91 Hsueh-Shih Road, Taichung, 40402, Taiwan*
[e] *Future Energy and Innovation Laboratory, Central European Institute of Technology, Brno University of Technology, Purkyňova 656/123, Brno, CZ-616 00, Czech Republic*
[f] *Department of Chemical and Biomolecular Engineering, Yonsei University, 50 Yonsei-ro, Seodaemun-gu, Seoul 03722, Korea*

mode of propulsion. In each section, the materials used for the propulsion of the robot and their role in the treatment of biofilms are described. Then, the removal of biofilms from infected indwelling medical devices using robots across different size scales is presented. Finally, we describe the applications implemented *in vivo* and *ex vivo* that show the proximity of the field of nano/micro/millirobotics to real-world applications.

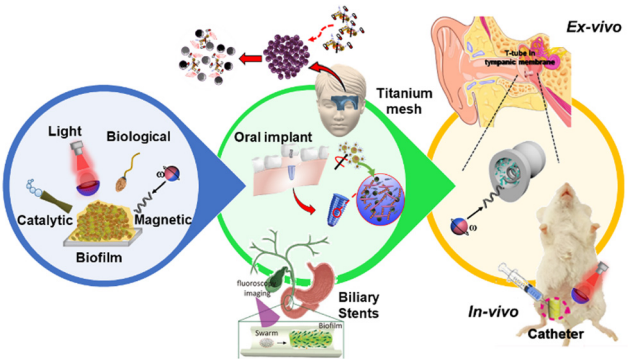

Fig. 1 Diagrammatic summary of this review. Different types of robots are used to disturb biofilms (left panel). Biofilm removal from infected indwelling medical devices (central panel). *In vivo* and *ex vivo* evaluation of biofilms treated by robotics at different size scales (right panel). Modified from ref. 49 and 56–59.

Carmen C. Mayorga-Martinez

Carmen Mayorga is currently a professor in the biomedical engineering undergraduate program at the Peruvian University of Applied Sciences (UPC). She served as a senior scientist at the Technical University of Ostrava and she held the position of Unit Leader and senior scientist at the Centre for Advanced Functional Nanorobots, UCT Prague. She was a research fellow in the nanobioelectronics and biosensors group/ICN2, Barcelona-Spain, and at Nanyang Technological University, Singapore. Her main research interests mainly include the development of bio/sensors based on 2D-material platforms functionalized with bioreceptors (enzymes, DNA, and antibodies) as well as micro/nano robotics at different scales and in different propulsion modes for biomedical applications and environmental monitoring. Moreover, she is also interested in the catalysis of 2D-materials for energy applications.

2. Biofilm structure, composition, and formation

A biofilm is a bacterial community encased in a sticky matrix of extracellular polymeric substances (EPSs),[24–26] playing a role in many persistent infections such as osteomyelitis, pulmonary infections in cystic fibrosis, dental plaques, urinary infections, ear infections, *etc.*[27] Moreover, biofilm formation is a strategy that microorganisms develop as a defense mechanism to survive under hostile conditions in the host and to obtain nutrients. However, bacterial biofilm formation is a major cause of human infections, and in many cases, it is associated with increasing antibiotic resistance. In addition, bacterial biofilms are responsible for infecting patients through indwelling medical devices.[28] Biofilm formation involves five stages that are schematized in Fig. 2: (i) reversible attachment of

Li Zhang

Li Zhang is a professor in the Department of Mechanical and Automation Engineering and a professor by courtesy in the Department of Surgery at The Chinese University of Hong Kong (CUHK). He is also a director of the SIAT-CUHK Joint Laboratory of Robotics and Intelligent Systems. Before joining CUHK as an assistant professor in 2012, he worked in Prof. Bradley Nelson's group as a postdoc and then as a senior scientist and lecturer in the Institute of Robotics and Intelligent Systems, ETH Zurich, Switzerland. Dr Zhang's main research interests include small-scale robotics and their applications in translational biomedicine.

Martin Pumera

Professor Martin Pumera is the Head of the Advanced Nanorobots and Multiscale Robotics Laboratory at Technical University Ostrava and Chief Investigator of Future Energy & Innovation Lab at CEITEC, Brno, Czech Republic. He founded the Center for the Advanced Functional Nanorobots at UCT Prague where he served as a director (2017–2023). He was a tenured group leader at the National Institute for Materials Science, Japan, in 2006. In 2010, Martin joined Nanyang Technological University, Singapore, where he worked as a tenured associate professor for almost a decade. Prof. Pumera has diverse research interests in nanomaterials and microsystems, in the specific areas of micro and nanomachines, quantum materials, machine intelligence and 3D printing.

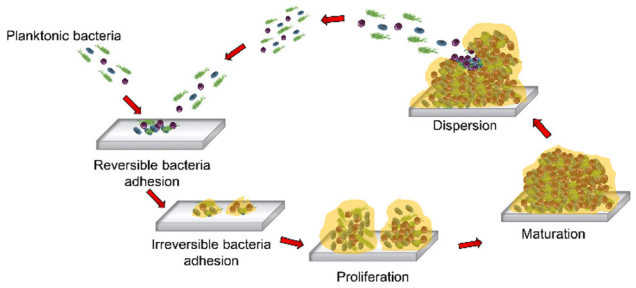

Fig. 2 Five stages of biofilm formation.

bacteria to a surface; (ii) irreversible attachment of bacteria; (iii) proliferation with microcolony formation; (iv) three-dimensional configuration of a bacterial community that settles down as a biofilm with cells replicating and EPSs accumulating; and (v) biofilm disassembling and bacterial detachment through dispersion in the fluid, leading to the formation of a new biofilm (Fig. 2).[29–32]

3. Propulsion modes of robots at different size scales for biofilm treatment

This section addresses the effect of the propulsion modes of micro/nanorobots, the importance of the materials used to prepare each one, and the role of both in biofilm disturbance. We divide this section into four subsections based on the propulsion mode, beginning with a description of catalytic micro/nanomotors followed by biological micromotors and micro/nanomotors powered by light illumination. Finally, we will describe robots driven by magnetic fields, which constitute the most widely used robots for bacterial biofilm removal.

3.1. Catalytically driven robots

Catalytic micro/nanomotors are propelled through the decomposition of a fuel using a catalyst. The catalyst can be a biological or inorganic agent. Enzymes, such as urease and catalase, are the most widely used biological catalysts while metallic platinum (Pt), silver (Ag), and MnO_2 are the most representative inorganic catalysts. Catalase, metallic Pt, and Ag produce O_2 and H_2O through the catalysis of H_2O_2, whereas urease catalyzes urea to form NH_3 and CO_2. In this sense, urea and H_2O_2 serve as the fuels.[33,34]

In 2020, the Pumera group developed biconical tubular catalytic micromotors of TiO_2, and Pt.[34] TiO_2 serves as the skeleton while Pt NPs provide the engine for the decomposition of H_2O_2. The mechanism of biofilm disruption is based on the synergistic interaction between H_2O_2, an antiseptic agent for treating oral biofilms (*e.g.*, *S. gordonii, V. parvula, F. nucleatum subsp. nucleatum*, and *A. naeslundi* bacterial strains), and the autonomous self-propelled TiO_2/Pt microrobots that require H_2O_2. In this context, the plausible mechanism of this biofilm treatment is based on (i) the continuous generation of O_2 bubbles, which may contribute to the mechanical disruption of the biofilm, and (ii) the generation of reactive oxygen species (ROS) by TiO_2 without light illumination, promotes the killing of bacteria. This simple mechanism has been shown to reduce bacterial viability up to 5% using 1% H_2O_2 during 5 min of treatment.[35]

Later in 2022, Quin *et al.* developed another tubular biconical micromotor based on tubular mesoporous silica (body) and MnO_2 inner layer (engine), decorated with ferromagnetic (Fe_3O_4) nanoparticles for magnetic control (see Fig. 3A). In these microrobots, mesoporous silica serves as the micromotor body and the MnO_2 inner layer (engine) acts as the catalyst to decompose H_2O_2 and generate oxygen bubbles (Fig. 3A(i)–(iii)).[36] Fe_3O_4 serves as the generator of ROS from H_2O_2 to destroy the bacteria biofilm and also functions as a magnetic guide. The mechanism of biofilm treatment is the same as in the previous work. The synergy of catalytic and magnetic actuation for propulsion enhances both mechanical disruption and reactive oxygen species (ROS) generation. In addition, magnetic micromotors can be guided through magnetic actuation to reach complex infection sites. The antibiofilm activity of these motors was evaluated against *S. aureus* and methicillin-resistant *S. aureus* (MRSA) bacteria strains. After the treatment of biofilms with Fe_3O_4–MnO_2 micromotors in the presence of 2 wt% H_2O_2 and under magnetic guidance, the residual viability of *S. aureus* and MRSA biofilms was reduced to 17.5%.[35] These results were further confirmed by 2D confocal images of residual biofilm bacteria using viable (green) and dead (red) bacteria staining through scanning electron microscopy as shown in Fig. 3A(iv) and (v), respectively. Similarly, Deng *et al.* developed an antimicrobial microrobot based on diatoms that load manganese oxide nanosheets with a polydopamine binder. These microrobots in the presence of hydrogen peroxide produce bubbles that penetrate the rigid and dense *P. aeruginosa* biofilm.[37]

Another approach developed by the Pumera group for biofilm treatment is based on paramagnetic microspheres modified with tosylated (sulfonyl esters) polystyrene, allowing the covalent bonding of indolicidin peptides.[38] To move the micromotor catalytically, microspheres are covered with a thin layer of Pt (Fig. 3B(ii)). The paramagnetic microspheres serve as the micromotor body while indolicidin peptides block bacterial DNA replication and Pt acts as the catalytic actuator (Fig. 3B(i)). A thin Pt layer with a thickness of 30 nm is sufficient to propel micromotors (Fig. 3B(iii)). After the biofilm treatment with peptide/PM/Pt microrobots in the presence of 0.5% H_2O_2, the viability of the MRSA biofilm decreased to 3.85%. 3D (top) and 2D confocal (bottom) images of residual biofilm bacteria using viable (green) bacteria staining confirm the efficient antibiofilm activity of peptide/PM/Pt microrobots (Fig. 3B(iv)).[38]

Another catalytic micromotor for biofilm removal discussed in this section is the one developed in 2021 by the Pumera group. In this work, the body of the micromotors is based on TiO_2/CdS nanotube bundles and the engine is urease (Fig. 3C(i)). These motors move in the presence of urea (Fig. 3C(ii)) and the TiO_2/CdS nanotube bundles function as a catalyst to generate ROS for killing bacteria. The efficiency of

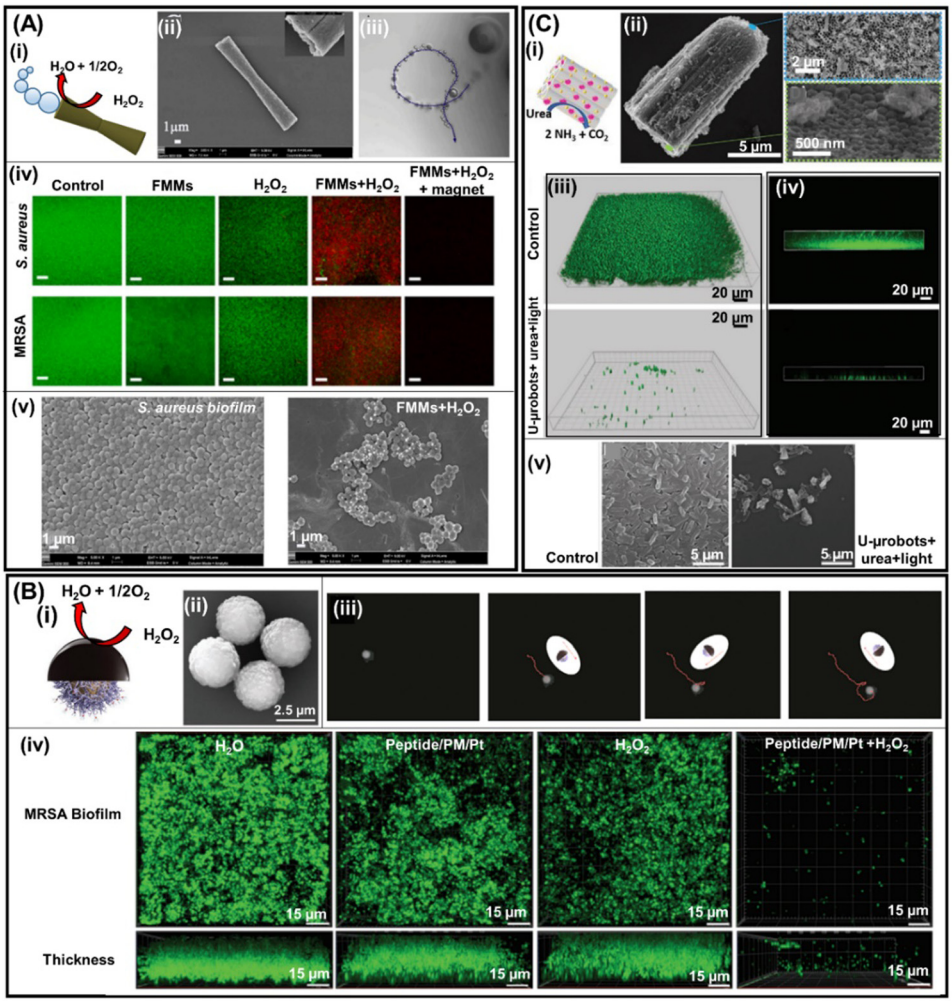

Fig. 3 Catalytic robotics for biofilm treatment. (A) Bubble-propelled FFM micromotors propelled by H_2O_2 (fuel) decomposition to O_2 and H_2O through the MnO_2 inner layer (i). SEM images of the FMMs and the inset illustrate its cavity (ii) as well as its swimming tracking line (iii). 2D confocal images of residual *S. aureus* (top panels) and MRSA (bottom panels) biofilm bacteria (iv) under different experimental conditions as well as SEM images of *S. aureus* biofilms untreated (left) and treated (right) with FMMs (v). Reprinted from ref. 36. (B) Diffusiophoresis mechanism, where the generation of O_2 is triggered by the catalytic decomposition of H_2O_2 on the surface of sputtered Pt (i), SEM image of the peptide/PM/Pt microrobots (ii), time-lapse tracked images of peptide/PM/Pt microrobot trajectories in the presence of 0.5 wt% H_2O_2 (iii). Confocal reflectance microscopy of the MRSA biofilm surface and thickness treated under different experimental conditions (iv). Reprinted from ref. 38. (C) Urease (engine) loaded on a TiO_2/CdS nanotube bundles microrobot propelled by the catalysis of urea, forming NH_3 and CO_2 (i). SEM image of a single urease/TiO_2/CdS nanotube bundles microrobot and its insets showing the end of open holes (top inset panel) and its opposite end (bottom inset panel) (ii). Confocal microscopy (iii) and (iv) and SEM images (v) of the biofilm before and after treatment with urease/TiO_2/CdS microrobots. Reprinted from ref. 39.

urease–TiO_2/CdS micromotors in eradicating biofilms was evaluated and the remaining bacterial viability was found to be around 20% (Fig. 3C(iii) and (iv)).[39] In this system, micromotors move, thanks to the urease (engine) that catalyzes urea, leading to the formation of NH_3 and CO_2, whereas TiO_2/CdS is an immotile photocatalyst.

Scarpa's group demonstrated that Nisin loaded on graphene oxide/platinum nanoparticles/Fe_2O_3 micromotors resulted in the efficient killing of *S. aureus* biofilms. The mechanism is based on the specific interaction of Nisin with the lipid II unit of *S. aureus*. Enhanced antibiofilm activity is observed when micromotors are catalytically propelled in the presence of H_2O_2 or by magnetic actuation using a permanent magnet.[40]

In summary, the performance of catalytic motors in eradicating biofilms was described in this section. The main advantage of these micromotors is that they do not need an external source for their propulsion. However, they require high concentrations of highly toxic fuels that cannot be found in the body under normal physiological conditions, which limits the possibilities for real-world applications.

3.2. Biological micromotors

Biological micromotors that are living, motile cells, *e.g.*, magnetotactic bacteria and sperm cells, are described in this section for efficient biofilm disruption. Here, the propulsion mechanism will be intrinsic to each cell and will be described

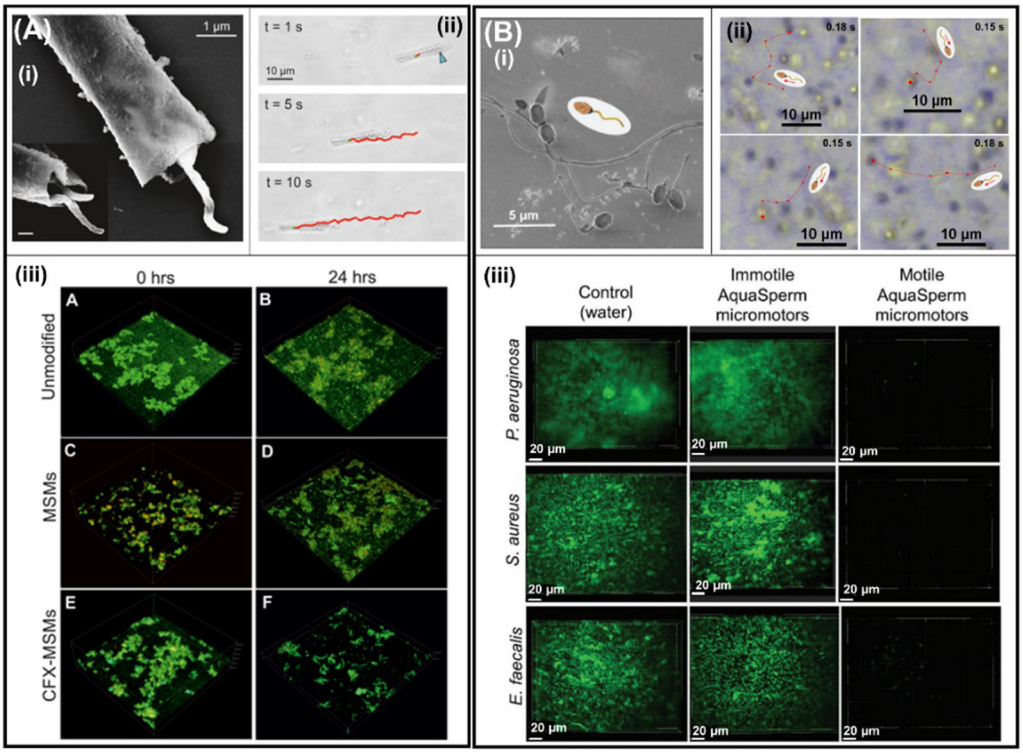

Fig. 4 Biological micromotors for biofilm treatment. (A) SEM of MSR-1 cells captured within a microtube; the inset shows an increased magnification of bacteria in the mesoporous silica microtube (MSM) (i). Bright-field microscopy images of MSR-1-powered biohybrid swimming. The blue arrow indicates the position of MSR-1 inside the microtube and the red track indicates the trajectory of the biohybrid (ii). 3D confocal images of live/dead cell staining of *E. coli* biofilms before (unmodified) and after treating with MSMs and ciprofloxacin-loaded MSMs (CFX-MSMs) (iii). Reprinted from ref. 41. (B) Scanning electron micrographs of catfish aqua sperm micromotors (i). Tracked microscopy images of aqua sperm micromotor trajectories after initiating mobility by adding ultrapure water (ii). 2D confocal images of *P. aeruginosa*, *S. aureus*, and *E. faecalis* biofilms before (control) and after treatment with immotile and motile aqua sperm micromotors (iii). Cells were stained with a SYTO 9 DNA probe. Reprinted from ref. 42.

accordingly. In 2017, the research groups of Sitti and Sanchez used the magnetotactic bacterium *Magnetospirillum gryphiswaldense* (MSR-1) as an engine to propel mesoporous silica microtubes loaded with antibiotics (ciprofloxacin (CPX)) to target and infect the biofilm of *E. coli* (Fig. 4(A)). These biological motors move by rotating their bipolar flagella and can self-generate magnetosome nanoparticles of Fe_3O_4. Moreover, they can be externally guided using an magnetic field. To produce biohybrid micromotors, MSMs, and MSR-1 are placed together, and gentle shaking is applied for 15 min. Once MSR-1 is inside MSMs (Fig. 4A(i)), the biohybrid micromotors exhibit continuous directional motion (Fig. 4A(ii)). In addition, biohybrid micromotors are magnetically guided. Antibiotic loading is possible due to the presence of nanoscale pores distributed throughout the tube body of the MSMs and its efficiency was first assessed using 3D confocal images (Fig. 4A(iii)). Once MSR-1 + CPX-MSMs were obtained, their antibiofilm activity was evaluated. After 24 h of treatment, no difference could be observed in *E. coli* biofilms treated with CPX-MSMs and MSR-1 + CPX-MSMs. However, the effect improved after 48 h and the MSR-1 + CPX-MSMs group showed a decrease in bacterial viability of 55%.[41]

Later in 2021, catfish aqua sperm cells (Fig. 4B(i)) were used to disturb the bacterial biofilm of *P. aeruginosa*, *S. aureus*, and *E. faecalis*. The disruption of the bacterial biofilm was due to the ultrafast speed of aqua sperm cells (114 ± 11 μm s^{-1}) when they came in contact with water (Fig. 4B(ii)). Fish sperm cells use water-induced dynein ATPase-catalyzed adenosine triphosphate (ATP) degradation as a biocompatible fuel to trigger their fast speed and snake-like undulatory locomotion, which is activated for less than 60 s. Moreover, the head size (Fig. 4B(i)) of aqua sperm micromotors facilitates their entry into the biofilm matrix. After the treatment of bacterial biofilms with ultrafast aqua sperm cells, the bacterial viability decreases compared with untreated biofilms or immotile aqua sperm cells, even in thicker biofilms grown for 48 h (Fig. 4B(iii)).[42] The greatest advantages of biological engines are their biodegradability and their abundance in nature. However, their biocompatibility is questionable as the introduction of non-human cells could lead to an allergic reaction or the pathogenicity of some bacteria strains. In this context, living cell-driven micro/nanomotors should adhere to the highest biocompatibility standards even when using genetically modified non-pathogenic bacteria; indeed, their toxicity should be thoroughly evaluated prior to pre-clinical trials (animals) and, furthermore, before initiating to human clinical trials. Moreover, aqua sperm micromotors lack controllable directionality. However, to avoid this disadvantage, Magdanz *et al.* developed biohybrid

magnetic microrobots by electrostatic self-assembly of immotile sperm cells and magnetic nanoparticles that can be manipulated by magnetic actuation.[43] This strategy would help direct the sperm micromotors towards biofilm removal but would require motile sperm. However, magnetotactic bacteria already self-generate magnetosome nanoparticles of Fe_3O_4 and are inherently controlled by the rotating magnetic field.

3.3. Light-driven robots

Light-driven robots are propelled by two mechanisms: light-induced physical effects and light-induced photocatalytic reactions.[40–42] Moreover, they are capable of wireless manipulation by modulating the light intensity and wavelength of light illumination.[44–46] In addition, light-induced photocatalytic reactions occurring in the presence of water or low concentrations of H_2O_2 are responsible for the propulsion of the robots and these reactions also generate reactive oxygen species (ROS) that can eliminate the bacterial biofilm.[47,48] For this reason, light-powered motors are very attractive for bacterial biofilm treatment. In 2020, the pioneering work led by X. Qu developed near-infrared (NIR) light-driven nanoswimmers (nanomotors) (see Fig. 5A(i)) that can penetrate *S. aureus* biofilms within 5 min and eradicate them through photothermal and antibiotic therapy. These nanomotors are composed of a mesoporous silica layer deposited on the SiO_2 shell used for vancomycin loading while Au nanoparticles are embedded on the inner side of the SiO_2 shell (Fig. 5A(ii)). The photothermal conversion of AuNPs triggers efficient NIR-driven nanomotors in different media (Fig. 5A(iii)). Biofilm removal by NIR-driven nanomotors is due to the synergistic effect of the localized thermal conversion generated by AuNPs that can destroy bacteria directly and, at the same time, induce the rapid release of vancomycin. This synergistic effect is noted in Fig. 5A(iv), where more than 90% of biofilm mass was destroyed.[49]

Later in 2021, Pumera *et al.* developed light-driven ZnO:Ag micromotors to eradicate *P. aeruginosa* and MRSA bacterial biofilms. The interesting round-shaped stars of ZnO:Ag microparticles were obtained by introducing silver precursors during the synthesis of ZnO (Fig. 5B(ii)). The propulsion mechanism is attributed to the enhanced photocatalytic activity of ZnO in the presence of Ag, which promotes light-driven self-electrophoretic motion in low H_2O_2 concentration under UV light illumination (Fig. 5B(i) and (iii)). However, the biofilm treatment is attributed to the ROS photogenerated on the ZnO:Ag micromotors as demonstrated in two bacterial strains, *P. aeruginosa* and MRSA (Fig. 5B(iv)).[50] Another material used for oral biofilm treatment is tubular black TiO_2/Ag nanorobots. These nanorobots can absorb a broad spectrum of light from

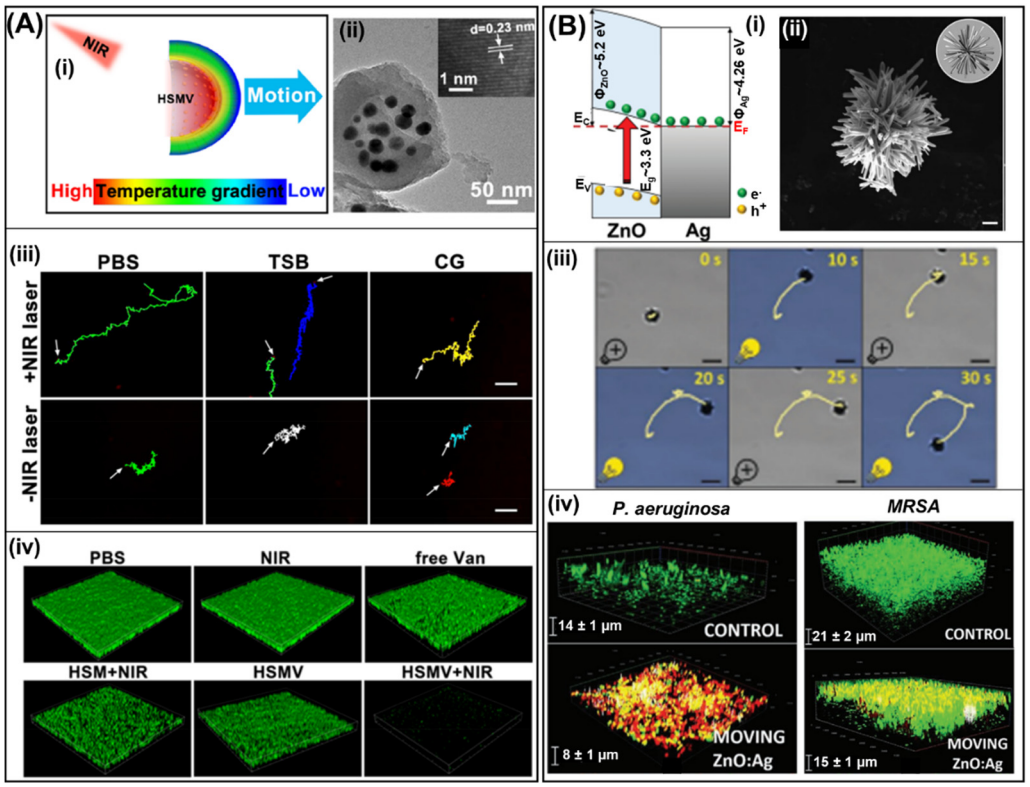

Fig. 5 Biofilm removal by light-driven microrobots. (A) Self-propulsion mechanism of HSMV upon exposure to a NIR laser (i). TEM image of the HSMV nanoswimmer as well as its high magnification lattice image (ii). Tracking line trajectories of HSMV in three different media in the presence and absence of laser irradiation (iii). Reprinted from ref. 49. (B) Electron-transfer mechanisms at the ZnO/Ag interface under UV-light irradiation. E_F: Fermi level; E_C: conduction-band energy level; E_V: valence-band energy level; E_g: optical bandgap; Φ_{Ag}: metal work function; and Φ_{ZnO}: semiconductor work function (i). SEM image of the ZnO:Ag micromotor (ii) tracked trajectories of the ZnO:Ag micromotor under light illumination and 1% H_2O_2 (iii). Live/dead 3D confocal images of residual *P. aeruginosa* (left) and MRSA (right) biofilms treated with ZnO:Ag micromotors (iv). Reprinted from ref. 50.

UV to the visible range which governs their multimodal motion. The interesting fast rotational motion of tubular black-TiO_2/Ag nanorobots decreases with increasing wavelengths. However, more effective biofilm removal was observed at 0.1% of H_2O_2 in the presence of UV light, reducing the total mass of the bacterial biofilm by up to 92%.[51]

In addition, UV light-driven amorphous, cubic, and tetrahedral Ag_3PO_4 micromotors are also explored for treating biofilms of Gram-positive and Gram-negative bacteria.[52] Interestingly, the inherent fluorescence of Ag_3PO_4 micromotors allows for their tracking and they can move under visible light illumination without the addition of H_2O_2 and can photogenerate ROS efficiently. Finally, it was demonstrated that the *P. aeruginosa* bacterial biofilm removal can be programmed by the shape of Ag_3PO_4 micromotors, with amorphous and tetrahedral micromotors being more efficient than cubic motors. However, superior performance in removing methicillin-resistant *S. aureus* biofilms is observed with micromotors and amorphous Ag_3PO_4 micromotors are more efficient than the tetrahedral and cubic versions.[52] The main advantage of light driven motors is that through light illumination, robots can be moved and at the same time bacteria are eradicated by the photoproduced ROS. However, ultraviolet light is very toxic. Moreover, UV, visible, and blue cannot penetrate muscle tissue deeply. In this regard, the most promising for future applications are nano/microrobots actuated by infrared light, the only wavelength that can penetrate muscle tissue deeply.

3.4. Magnetically driven robots

Magnetic micro/nanomotors are powered by magnetic fields that originate from the movement of an electric charge as vector functions of position and can be generated by freely moving electric currents and magnetic materials.[3] Usually, the moving electric current source is generated by the coil of an electromagnet and is externally controllable. These motors are fully maneuverable, wireless, and can reach confined places; hence, these micro/nanorobots are very promising structures for eradicating biofilms that develop in difficult-to-access and complex, confined spaces.[3,4,53] The pioneering work using magnetic robots was reported by H. Koo *et al.* in 2019. They developed catalytic antimicrobial robots (CARs) for efficient *S. mutans* biofilm treatment. CARs are based on iron oxide nanoparticles that allow their magnetic propulsion and generate bactericidal free radicals in the presence of 1% H_2O_2, which can break down the biofilm matrix and remove the fragmented biofilm debris residues using enzymes (dextranase/mutanase), preventing the reinitiation of the biofilm life cycle. CARs are actuated *via* magnetic displacement, achieved by placing a permanent magnet below the NP suspension. The efficient biofilm removal of CARs in the presence of H_2O_2 and enzymes is evaluated. This method initially involves catalysis-mediated biofilm disruption by the iron oxide nanoparticles and H_2O_2. Next, the magnetic actuation to pull out the biofilm from the colonized surface using CARs is observed. Finally, 24 h of incubation completes the degradation of fragmented biofilm debris by enzymes, resulting in neither viable bacteria nor biofilm regrowth.[54]

Later, L. Zhang's group implemented a magnetic microswarm of porous Fe_3O_4 mesoparticles (Fig. 6A(ii) and (iii)) actuated by a rotating magnetic field (Fig. 6A(i) and (iv)). The efficient eradication of *E. coli* and *B. cereus* biofilms by the p-Fe_3O_4 swarm is attributed to two factors: the toxic free radicals generated by the Fenton reaction to kill bacteria and the mechanical disruption produced by the microswarm motion that promotes the penetration of free radicals in the matrix of the biofilm as can be seen in 3D confocal images (Fig. 6A(iv)). In addition, it was demonstrated that the higher free radical production, attributed to the porous structure of Fe_3O_4, decreases the relative bacterial viability to 0.3% and 0% for *E. coli* and *B. cereus*, respectively.[55]

Another approach developed by Mayorga-Martinez *et al.* to eradicate bacterial biofilm involves the use of a photocatalyst decorated with ferromagnetic nanoparticles (Fig. 6B(i)). In this work, the photocatalyst (B_iVO_4 microparticles, see Fig. 6B(ii)), photo-generated ROS, and ferromagnetic nanoparticles (Fe_3O_4 nanoparticles, see Fig. 6B(iii)) promoted magnetic actuation (Fig. 6B(iv)). These hybrid micromotors are used to eradicate oral biofilms composed of three known supragingival plaque bacteria (*S. gordonii*, *A. naeslundii*, and *V. parvula*). This approach also demonstrated that the synergistic effects of both free radical production and mechanical forces generated by magnetic propulsion reduce biofilm viability by up to 93% (see fluorescence and 2D confocal images presented in Fig. 6B(v)).[56] Moreover, the strong mechanical forces generated by Fe_3O_4@PEI/$BiVO_4$ magnetic microswarms are responsible for efficient biofilm disruption, which is not observed when using lone $BiVO_4$ microparticles propelled by light illumination or magnetic field. For this reason, the greatest contribution to the mechanical forces generated by these microrobots is due to magnetic actuation, while light illumination serves to generate ROS to eliminate bacterial biofilms.

Magnetic urchin-like capsule robots (MUCRs) obtained from pitted natural sunflower pollen (see Fig. 7A(i)) were used to eradicate *E. faecalis* and multidrug-resistant *E. coli* (MREC) bacterial biofilms. MUCRs were loaded with magnetic liquid metal droplets (MLMDs) (see TEM images on the right side of Fig. 7A(i)) and a chemotactic agent (L-aspartic acid). Individual MLMD robots show controlled locomotion under the rotating magnetic field (Fig. 7A(ii)). However, under the guidance of an external magnetic field, MLMD robots generate a swarm that navigates on a flat surface along a predesigned curved trajectory (Fig. 7A(iii)), thereby disrupting the biofilm more efficiently than a single unit of MLMDs. The biofilm removal mechanism of the MLMD swarm is based on (1) the synergistic effect of releasing sharp MLMDs to kill bacterial cells, (2) the chemotactic agent that captures them, and (3) chemotaxis attraction to devastate the planktonic bacteria released from the biofilm by the mechanical disruption of the biofilm by microswarms of MUCRs (Fig. 7A(iv)).[57]

Another magnetic microrobot developed to eradicate bacterial biofilms efficiently was reported by Mayorga-Martinez *et al.*

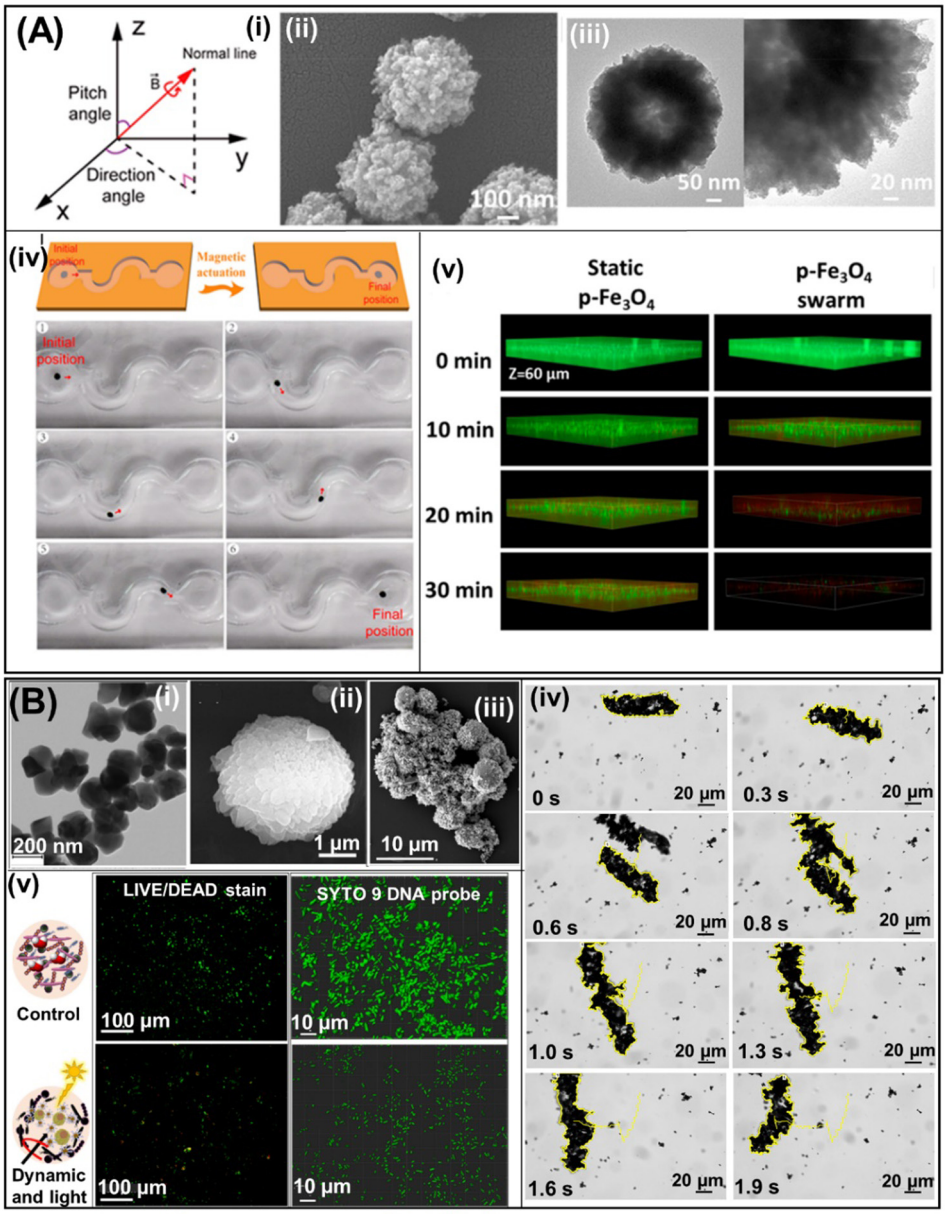

Fig. 6 Magnetic robots for biofilm treatment. (A) Diagram of the rotating magnetic field produced by the electromagnetic coil system (i). SEM and TEM images at different magnifications of p-Fe_3O_4 MPs (ii) and (iii). Schematic representation and photograph of the p-Fe_3O_4 swarm's steering in an S-shaped channel (red arrow indicates the swarm's direction of movement) (iv). 3D confocal micrographs of *E. coli* biofilms treated using static p-Fe_3O_4 (left) and the Fe_3O_4 swarm (right) at different times (iv). Reprinted from ref. 55. (B) SEM images of Fe_3O_4@PEI/$BiVO_4$ magnetic microrobots (i), $BiVO_4$ microparticles (ii), and Fe_3O_4@PEI (iii). A time-lapse microscopy image illustrating tracking lines of a Fe_3O_4@PEI/$BiVO_4$ magnetic microrobot swarm under a transversal rotating magnetic field (iv). Bacterial viability visualization using live/dead stain under fluorescent illumination (left), SYTO 9 DNA probe in fixed samples, and confocal microscopy (right) of biofilms before and after treatment with Fe_3O_4@PEI/$BiVO_4$ photoactive magnetic microrobots (iii). Reprinted from ref. 56.

These microrobots are composed of halloysite nanotubes (HNTs) as the backbone and iron oxide (Fe_3O_4) nanoparticles as magnetic actuators. They are covered with polyethylenimine (PEI) to load ampicillin and potentiate its antibiotic activity as well as to prevent the disassembly of microrobots. SEM images (Fig. 7B(i)) of each component are represented in Fig. 7B(i): Fe_3O_4 NPs (top panel), and HNTs (central panel) and Fe_3O_4-HNT/PEI microrobots (bottom panel). Moreover, this microrobot can be magnetically actuated to exhibit different motion modes (*i.e.*, tumbling and spinning) or combined motion modes (Fig. 7B(ii) and (iii)). Moreover, they can self-organize into swarms and form a ribbon or vortex when they are actuated in a tumbling or spinning mode, respectively. These swarms can be transformed from ribbon to vortex and *vice versa*. Finally, efficient biofilm disruption is demonstrated by a reduction in bacterial viability of four orders of magnitude

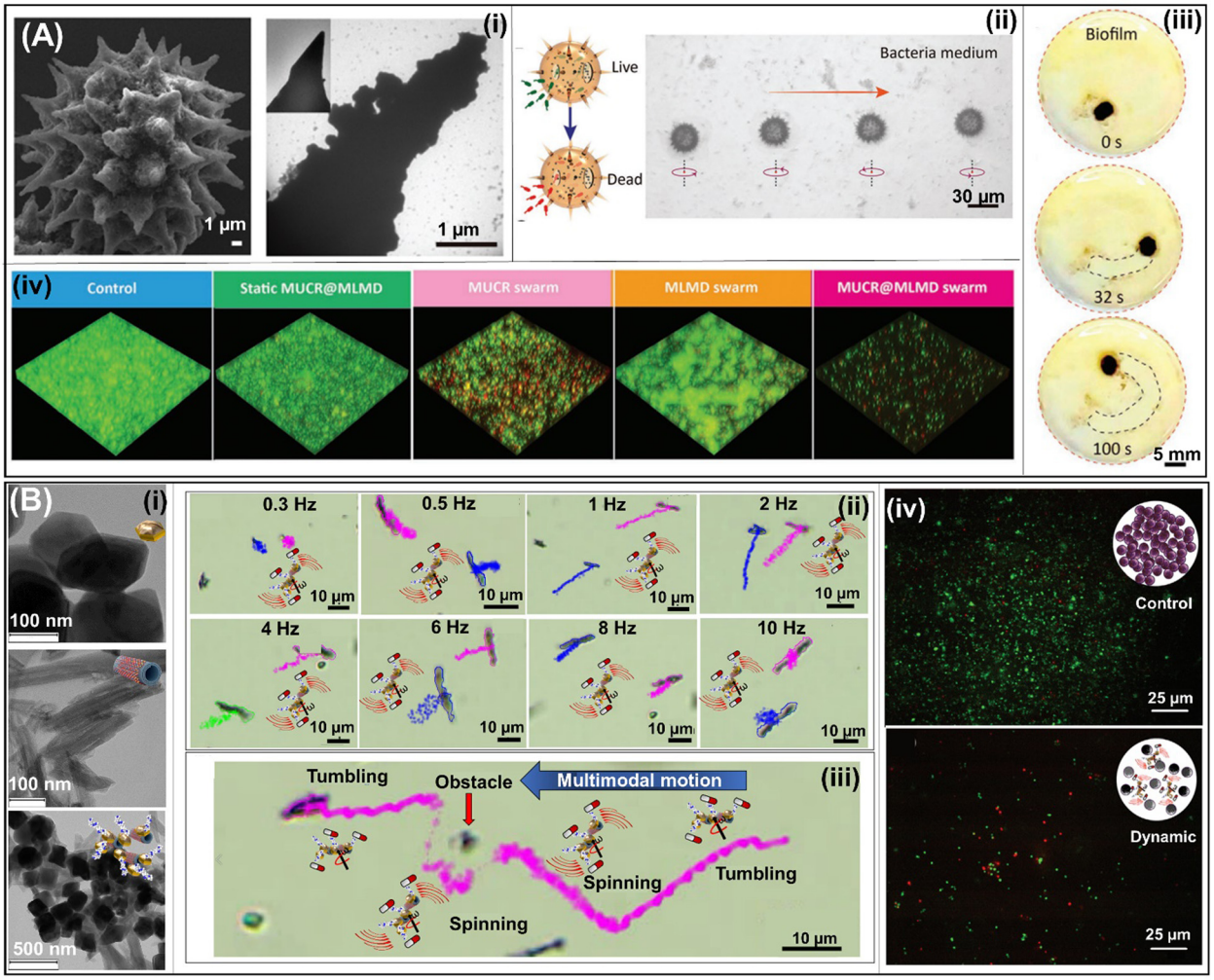

Fig. 7 Magnetic robots for biofilm treatment. (A) SEM image of the MUCR obtained after chemical bath deposition and the magnified TEM image of the individual spines of MUCRs (i). Schematic and snapshots depicting a microrobot dynamically spinning through a bacterial medium, effectively eliminating bacteria. (ii). Swarm generated by many MLMD robots under a magnetic field that navigates on a flat surface along a predesigned curved trajectory, disrupting bacteria biofilms (iii). 3D live/dead confocal images of MREC biofilms under different treatments (iv). Reprinted from ref. 57. (B) TEM images of each component of Fe_3O_4-HNT/PEI magnetic nanorobots. Top: Fe_3O_4 NPs; central: HNT; and bottom: Fe_3O_4-HNT/PEI (i). Time-lapse optical microscopy images of tracking lines of spinning motions of individual magnetic Fe_3O_4-HNT/PEI@Amp microrobots at different frequencies (ii) as well as multimodal motion of individual magnetic Fe_3O_4-HNT/PEI@Amp microrobots from tumbling to spinning and from spinning to tumbling at 1 Hz, and its ability to avoid an obstacle (iii). Bacterial viability visualization by fluorescence microscopy of live/dead-stained intact biofilms (top panel) and biofilms treated with dynamic magnetic microrobots (bottom panel) (iv). Reprinted from ref. 58.

(Fig. 7B(iv)). The impressive performance of these microrobots in eradicating bacterial biofilms is attributed to (i) the mechanical forces generated by the magnetic propulsion, allowing their penetration into the biofilm matrix, and (ii) the enhanced antibacterial activity of the antibiotic by the PEI (β-lactam potentiator).[58]

Recently, a graphene oxide (GO) Fe_2O_3 helical micromachine (HMM) was reported to show peroxidase-mimicking activity, generating ROS for biofilm removal.[58] The magnetic actuation of the Fe_2O_3 HMM is generated by a moving spherical permanent magnet carried by a 6-DOF robotic arm that can be easily maneuvered along a tube. Efficient biofilm mechanical removal is demonstrated by rolling the Fe_2O_3 HMM on a planar surface previously colonized by methicillin-resistant *S. aureus* (MRSA) bacteria. The result displays a clear decrease in biofilm thickness after treatment with the Fe_2O_3 HMM in the presence of H_2O_2 actuated by the rotating magnetic field, benefiting from a combination of mechanical forces and the effect of ROS generated by the catalysis of H_2O_2.

Magnetic robots with different sizes and shapes are probably the most promising structures for eradicating bacterial biofilms. If we start from the fact that the mechanical forces generated during their motion disrupt the biofilm matrix, then a significant portion of the work is accomplished. These robots can transport different antibacterial agents, such as antibiotics, chemotactic, β-lactam potentiators, and photocatalysts, to produce ROS and ensure almost complete biofilm removal. Specifically, for magnetic actuation, it is necessary to integrate

Table 1 Summary of pros and cons of biofilms treated with multiscale robots with different propulsion modes

Propulsion mode	Pros	Cons
Catalytic	No need for an external source, synergistic antibacterial activity with the fuel (H_2O_2), generation of strong mechanical forces	Toxic fuel, no motion control, limited biocompatibility by the fuel and materials used for their manufacture, low biodegradability, and limited multimaterial integration
Biological	No need for an external source, naturally available, fuel-free, and biodegradable; generation of strong mechanical forces	Limited biocompatibility (pathogenicity and allergen), no motion control, limited multimaterial integration
Light	ROS generation, fuel-free or low concentration of fuel	Need external source of light, no motion control, does not generate strong mechanical forces, non-biodegradable, limited biocompatibility, limited multimaterial integration
Magnetic	Total motion control, fuel-free, generation of strong mechanical forces, easily integrated with different materials	Need bulky and complicate magnetic control, non-biodegradable, limited biocompatibility

magnetic materials into the body of the micro/nanorobots, which are mostly not biodegradable or biocompatible. In addition, magnetic actuation requires bulky and complicated auxiliary control equipment.[60] However, the magnetic material (*i.e.*, Fe_3O_4) possesses intrinsic catalytic properties, generating ROS,[61] as well as a strong magnetic hyperthermal capacity,[62] which were used to efficiently treat bacterial biofilms.

In this section, we have described and discussed different milli/micro/nanorobots used to treat bacterial biofilms. Table 1 summarizes the advantages and disadvantages of each kind of robot used. Among the most notable antibacterial mechanisms for this purpose was the generation of mechanical forces by their propulsion, enabling them to disrupt and penetrate the EPSs of the biofilm. Magnetic robots are the strongest force generators, followed by biological and catalytic motors. Moreover, magnetic robots can fully control their direction and can reach confined spaces. However, the directionality of the other motors can be controlled by adding magnetic materials to their structures. On the other hand, most of the engines described were manufactured using synthetic inorganic micro/nanomaterials, limiting their biodegradability and probably their biocompatibility. For this reason, biodegradability and biocompatibility have to be studied exhaustively before progressing to animal and clinical trials. Hence, it seems that combining smart materials with antibacterial activity and motion capability to generate strong mechanical forces is the best strategy for treating bacterial biofilms.

4. Biofilm removal from infected indwelling medical devices

Indwelling medical devices are used in hospitalized and non-hospitalized patients. However, the prolonged presence of medical devices within the body heightens the susceptibility to bacterial infections due to the persistent formation of biofilms. This can lead to increased medical expenses associated with the treatment or removal of the indwelling device.[63–66] Nevertheless, robots have enormous potential to treat bacterial biofilms that colonize indwelling medical devices. In this section, we will describe how biofilms can be eradicated from the surface of implants and catheters. However, it should be noted that here we will focus particularly on the applications carried out *in vitro* at the laboratory level.

4.1. Biofilm removal from metallic implants

Medical implants placed inside or on the surface of the body are designed to replace a missing biological structure, support a damaged biological structure, or enhance an existing biological structure. They are made from metal (titanium), ceramics, silicone, or apatite.[67,68] However, regardless of the purpose of the implant, it must be free of infections to ensure its effectiveness in the applied medical treatment.[69,70]

In particular, dental implants placed in the jawbone provide a foundation for oral prosthetics (*e.g.*, crowns, bridges, and dentures) or a broader facial prosthesis. Peri-implantitis is gum inflammation caused by oral biofilms, which consists of a complex mixture of several species of oral bacteria and is the most common complication in dental implantology. However, if the infection is not properly treated, then the inflammation can spread to the bone next to the implant, causing its rejection in most cases.[71–74]

Starting from this premise, Pumera's group used photocatalytic magnetic microrobots (see Section 3.4) composed of $BiVO_4$ (photocatalyst) and Fe_3O_4 (magnetic actuator) for the removal of oral biofilm-infected titanium implants through the synergistic effect of mechanical forces generated by magnetic actuation and the photogeneration of ROS (Fig. 8A). For this purpose, an osseo-integrated implant (implant 1) and an abutment (implant 2) infected with a mixture of oral biofilms of *S. gordonii*, *V. parvula*, *A. naeslundii*, and *F. nucleatum* were then treated with photocatalytic magnetic microrobots. It was clearly demonstrated that bacterial viability reached 50% and 88% for implant 1 and implant 2, respectively (Fig. 8A, right panel).[56] Later, the same group demonstrated biofilm treatment using light-driven tubular black-TiO_2/Ag nanorobots (see Section 3.3) from a facial titanium implant used for jaw restoration (Fig. 8B). The efficient ROS photogenerated by black-TiO_2/Ag nanorobots under UV light illumination is responsible for the biofilm removal and decrease in bacterial viability by about 50% (Fig. 8B, right panel).[51]

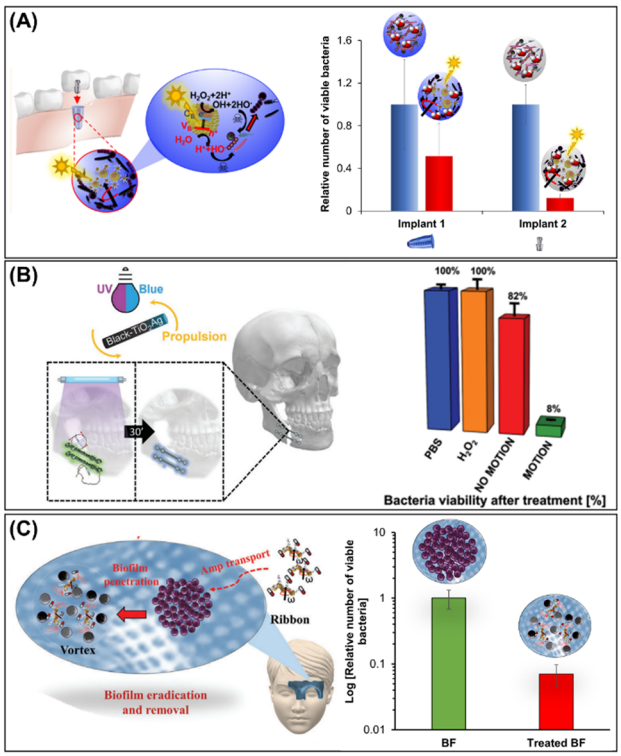

Fig. 8 Biofilm removal from implants. (A) Schematic representation of oral biofilm treatment from the intraosseous implant (implant 1) and abutment (implant 2) using photoactive Fe_3O_4@PEI/$BiVO_4$ magnetic microrobots and the antibacterial activity against mixed oral biofilms (*S. gordonii, V. parvula, A. naeslundii,* and *F. nucleatum*) colonization. Reprinted from ref. 51. (B) Light-driven self-propelled tubular B-TiO_2/Ag nanorobots to eradicate multispecies biofilm from facial titanium miniplates (left panel) used in maxillofacial surgery and their antibiofilm activity (right panel). Reprinted from ref. 56. (C) Schematic representation multimodal motion in the swarm mode, and antibacterial activity of HNT-Fe_3O_4@PEI/Amp microrobots for the removal of *S. aureus* biofilm colonized on titanium mesh used for bone restoration. Reprinted from ref. 58.

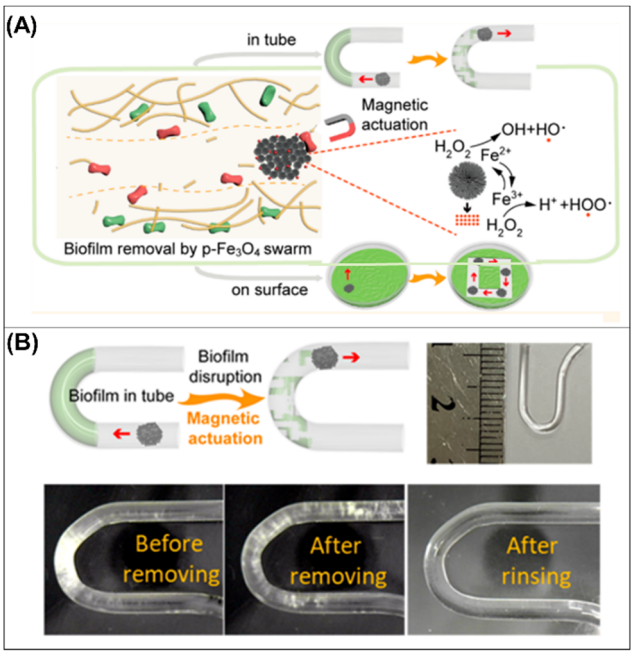

Fig. 9 Biofilm removal from medical catheters. (A) Schematic diagram of the synergic effect of chemical and mechanical forces for bacterial killing by p-Fe_3O_4 MPs in a swarm mode motion (A). Schematic diagram (top and left panels) and digital photographs (bottom panels) of biofilm disruption in a tiny U-shaped tube by a dynamic Fe_3O_4 swarm as well as an optical image of a U-shaped tube (top and right panel) (B). Reprinted from ref. 55.

The major disadvantage of biofilm treatment through ROS photogeneration is that UV-vis light cannot penetrate deeper tissue. Dental and maxilla facial implants are placed in the gums and covered with a keratinized epithelium through which light can penetrate very easily. Nevertheless, UV light can be toxic to the human body. To address these issues, Mayorga *et al.* developed another approach to treat biofilms on the titanium mesh used for facial bone restoration placed under tissue depth (Fig. 8C). This system was based on HNT microrobots decorated with magnetic particles and coated with PEI and ampicillin. These microrobots were able to decrease biofilm viability by up to two orders of magnitude, resulting in 93% biofilm removal.[58]

4.2. Biofilm colonized on medical catheters

Medical catheters are thin tubes with different levels of stiffness depending on the application and functionality. They can be inserted in the human body to complete a therapy or perform a medical procedure. However, bacterial colonization of catheter surfaces is responsible for the majority of healthcare-associated infections (HAIs).[75–77] HAIs can lead to the death of the patient or cause the rejection of an indwelling device. For this reason, the early and effective treatment of the biofilm that colonizes indwelling catheters is necessary in order to safeguard the lives of patients as well as avoid unnecessary surgical costs to remove expensive catheters.

In this context, robots emerge as a promising solution, particularly due to their accurate manipulation by magnetic fields, allowing them to be perfectly manipulated along the tube from one end to the other and back again. In addition, the mechanical forces generated by magnetic propulsion are strong enough to remove bacterial biofilms very easily. This was demonstrated by Koo's group in 2019, where the magnetic robots, called CARs, mechanically destroy the biofilm tightly attached to a catheter.[54] Later, Zhang *et al.* demonstrated that tiny microrobots comprising Fe_3O_4 mesoparticles can mechanically and efficiently remove biofilms colonized on a catheter when they move together in a swarm mode under magnetic actuation (Fig. 9(A and B)). Both robots eliminate bacterial biofilms through the catalytic generation of ROS in the presence of H_2O_2.[55]

Mayorga-Martinez *et al.* demonstrated that the mechanical forces generated by the ultrafast aqua sperm micromotors from catfish efficiently destroy the biofilm formed by different bacteria that colonized catheters. This approach has several advantages such as a fast treatment time (less than 1 min), biocompatible fuel (water), and the abundance of micromotors as a fish produces millions of them. However, its main

disadvantage is instability because fish sperm are efficient only for a few days after extraction from the gonads. Therefore, it is imperative to develop protocols for the long-term preservation of sperm to ensure sperm efficacy. It is also necessary to study the safety of sperm in the body to prevent the activation of an immune response.[42]

5. *In vivo* and *ex vivo* biofilm treatment using robots of different sizes

Modern wireless robots offer countless applications in the biomedical field. However, multiscale robot investigations carried out *in vivo* or *ex vivo* are the most relevant because they provide a closer approximation to real-world scenarios. It is a great challenge to investigate multiscale robots for biofilms treated in a living body (*in vivo*) or in an organ system studied *ex vivo*.

Despite the advances made in recent years in the use of milli/micro/nanorobots for the treatment of bacterial biofilms, a thorough study of a living organism is still needed as it is debatable whether *in vitro* biofilms actually resemble *in vivo* biofilms. Recent reports in animal models showcasing their use for treating bacterial infections demonstrate their effectiveness.[78–80] However, in the case of the treatment of bacterial biofilms, the studies carried out are still few. In 2019, Qu *et al.* demonstrated biofilm removal *in vivo* from catheters infected with *S. aureus* by using near-infrared (NIR) light-driven nanomotors. As explained before, these nanomotors disrupt *S. aureus* biofilms by the photothermal conversion of asymmetrically distributed AuNPs in the functionalized mesoporous silica half-shell motor loaded with vancomycin (HSMV) (see Section 3.3). The pre-infected catheters were implanted subcutaneously in anesthetized mice followed by the subcutaneous injection of HSMV and NIR light irradiation (Fig. 10A). After NIR irradiation, the temperature increased to 45 °C compared with control experiments, which can be seen from thermographic images (Fig. 10B(i)). In addition, wound sizes of mice decreased significantly in the treatment group with HSMV + NIR irradiation compared with the control groups; indeed, wounds exhibited scab formation and even complete healing after 7 days (Fig. 10B(ii) and (iii)). In addition, tissue around the implanted site was evaluated through histological analysis; little cell debris and few tissue lesions were observed in mice treated with HSMV + NIR, confirming wound healing (Fig. 10(iv)). Finally, the remaining bacteria in the implanted catheter were inspected by scanning electron microscopy (Fig. 10B(v)), and the complete absence of bacteria was observed in the group treated with HSMV + NIR irradiation nanomotors. The results obtained in this paper demonstrated the promising real-world applications of nano/microrobots for biofilm treatment that can be implemented in medical practices.[49]

A few years later, Zhang's group used Fe_2O_3 HMM magnetic robots described in Section 3.4 to remove biofilms from an infected tympanostomy tube (T-tube) inserted in the tympanic

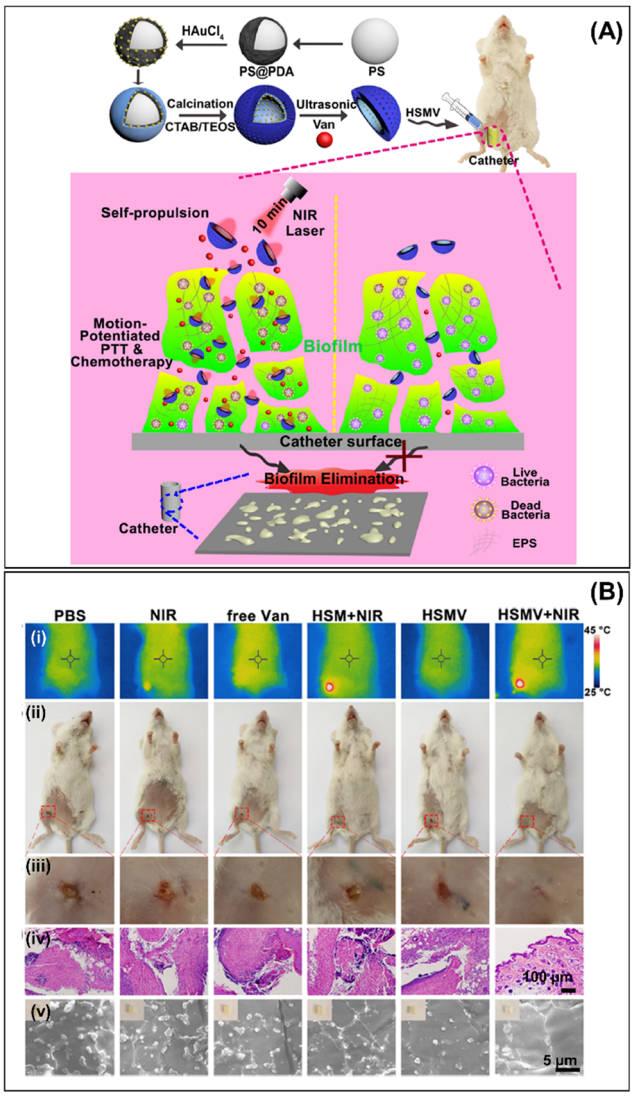

Fig. 10 *In vivo* biofilm removal. (A) Schematic illustration of HSMV nanoswimmer synthesis (top panel) and motion-enhanced synergistic antibiofilm therapy upon laser irradiation in the catheter indwelled in mice leg (bottom panel). (B) Results of *in vivo* antibiofilm efficacy of HSMV nanoswimmer evaluated using a mouse implant-related periprosthetic infection model. (i) Thermographic images, (ii) digital photographs and their magnified images of the incision site (iii), (iv) histological photomicrographs of skin tissue around the implanted site, and (v) SEM images of embedded catheters in infected mice treated with PBS, NIR, free Van, HSM under laser irradiation, HSMV, and HSMV under laser irradiation. Reprinted from ref. 49.

membrane of a human cadaver (*ex vivo*) (Fig. 11A). A magnetic Fe_2O_3 HMM and H_2O_2 were delivered in the T-tube using an ENT endoscope. Next, a rotating magnetic field was applied to actuate the Fe_2O_3 HMM (Fig. 11B(i) and (ii)). The efficient treatment was possible due to the synergistic effect of mechanical forces generated by the magnetic propulsion of HMM and the ROS generated by the decomposition of H_2O_2 through Fe_2O_3 (Fig. 11B(iii)). After treatment, the Fe_2O_3 HMM was retrieved using a tiny bar magnet (Fig. 11B(iv)). The presence of bacterial biofilms in the patient's infected T-tube was investigated before treatment and visible living bacteria were

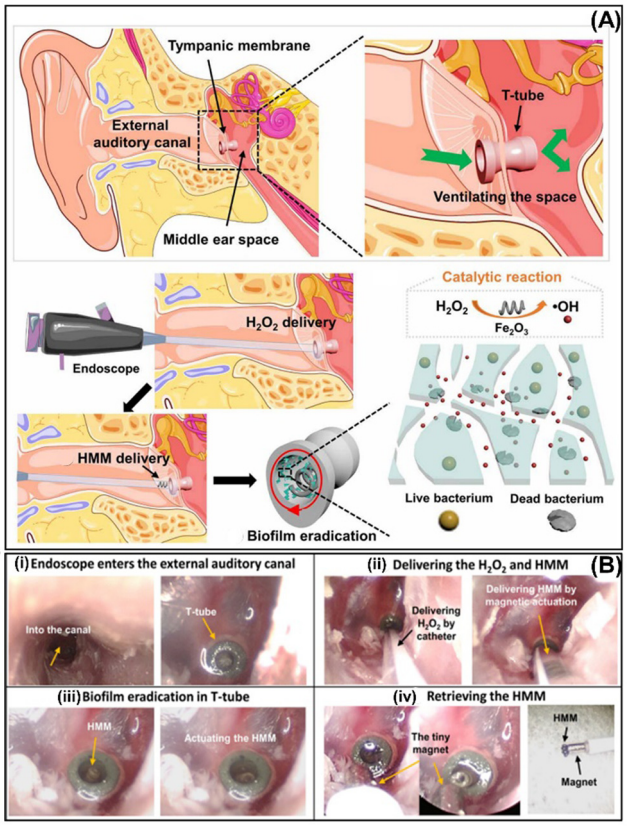

Fig. 11 (A) Endoscope-assisted magnetic helical micromachine delivery for biofilm eradication in the tympanostomy tube (T-tube). (B) The treatment procedure for biofilm in the infected T-tube from a cadaver head (i) using magnetic Fe_2O_3 HMM and H_2O_2 delivered using an endoscope (ii), magnetic actuation inside of T-tube (iii), and its retrieval (iv). Reprinted from ref. 59.

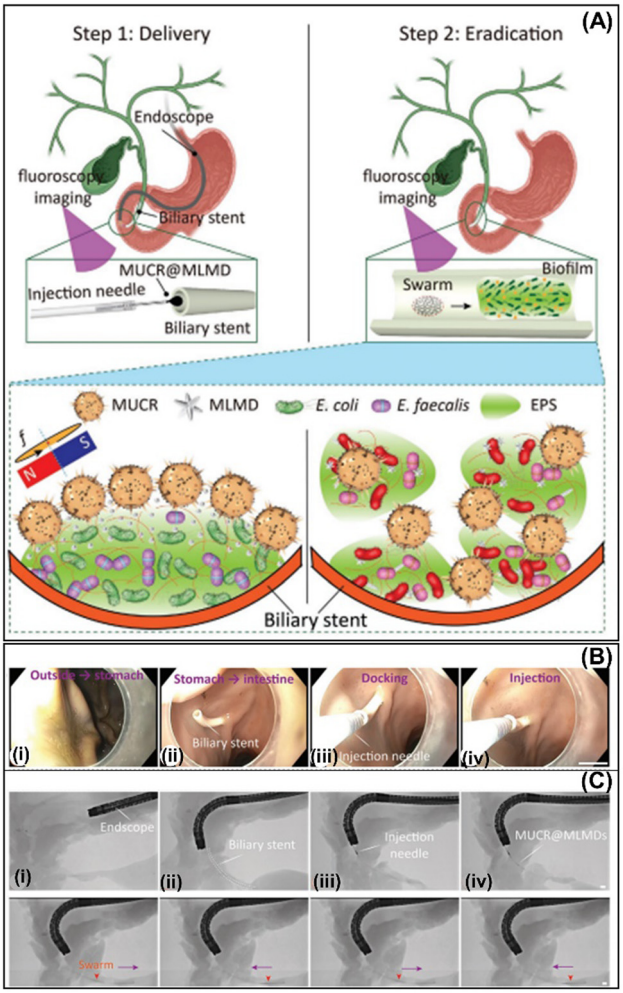

Fig. 12 Magnetic microswarms for biofilm eradication in biliary stents. Schematic diagram of the treatment of the biofilm adhered to biliary stents using the MUCR@MLMDs swarm (A). An injection needle equipped with the endoscope delivers the microswarm into the biliary stents (B) and images are taken by endoscopy and fluoroscopy imaging (scale bars: 5 mm) (C). Reprinted from ref. 57.

observed. However, after treatment, almost complete biofilm removal was confirmed.[59]

In addition, Zhang's group treated biofilm-associated pathogen infections on inaccessible biliary stents using magnetic urchin-like capsule robots (MUCRs) loaded with magnetic liquid metal droplets (MLMDs) and l-aspartic acid as described in Section 3.4. Biliary stents are tiny tubes used to prevent obstruction during endoscopic retrograde cholangiopancreatography (Fig. 12A). The biofilm formation on the stent lumen surface blocks and subsequently clogs it. In this study, biliary stents that had been indwelling in patients for about 2–3 months were collected and then surgically inserted at the junction of the duodenum and bile duct of fresh gastrointestinal and biliary systems of pigs. After that, MUCR@MLMDs microrobots were injected directly with an endoscope, followed by the application of magnetic actuation (Fig. 12B). The microrobots' navigation and biofilm removal in the biliary stents were tracked by fluoroscopy imaging (Fig. 12C). After 30 min of treatment, the clean inner wall of biliary stents was observed.[57]

Finally, Oh *et al.* introduced surface topography-adaptive robotic superstructures (STARS), which are used for the chemical treatment and mechanical removal of adhesive biofilms, and multiplexed pathogen detection by capturing bacterial, fungal, viral, and matrix components. STARS utilize Fe_3O_4 NPs and use automated motion patterns to reach complex three-dimensional geometries of *ex vivo* human teeth. STARS mimic "toothbrushing-like" and "flossing-like" motions to remove the biofilm in real-time while capturing samples with microscale precision for multikingdom pathogen detection.[81] Moreover, this group also demonstrated that catalytic Fe_3O_4 NPs assembled into microswarms or embedded in soft helicoids under magnetic fields can be controlled to disrupt and capture biofilms inside the root canal of teeth in an *ex vivo* model.[82]

Conclusions and outlook

In recent years, great innovations have emerged in the treatment of bacterial biofilms using different milli/micro/nanorobots, including innovative manufacturing approaches with high antibacterial activity as well as smart materials for their

motion, shape reconfiguration, programmable navigation, and clinically oriented approaches. In this tutorial review, we described all the current strategies implemented for the treatment and removal of bacterial biofilms using robots at different scales. In addition, we systematically described the robots used and grouped them according to their mode of propulsion. Moreover, a critical analysis of the advantages and disadvantages of each type of robot used in the treatment of biofilms was conducted. As can be seen, robots of different sizes and shapes are promising tools for the eradication of bacterial biofilms that colonize different medical devices and implants. The initial engines exhibited limited antibiofilm activity, with an efficiency of less than 90%. However, they have evolved to reach reported eradication rates up to $\geq$99%, particularly in the case of multifunctional robots that combine intelligent materials for both actuation and bacterial biofilm eradication. This includes using ROS-generating catalytic nanomaterials ($BiVO_4$, TiO_2, ZnO/Ag, Ag_3PO_4, Fe_3O_4, *etc.*) as well as robots that can load indolicidin peptides or antibiotics. Incipient applications implemented *in vivo* and *ex vivo* demonstrate their potential for use in real applications. However, it is necessary to conduct more in-depth studies on the biodegradability and toxicity in the human body of robots to verify that they do not cross the barriers of the organism or accumulate in cells, leading to acute or chronic toxic effects. Another concern that must be considered is the large-scale production of the materials used to manufacture the robots. Taking into account not only the cost of precursors but also the apparatus used, this approach has the potential to provide real economic and social benefits. It is imperative to keep these considerations in mind from the beginning of the design of these dynamic devices. Finally, the precise maneuvers of the robots in the body and in real-time are very important for their monitoring and to guarantee that the robots are located at the infectious focus where the bacterial biofilm is developing. Most of the *in vivo* and *ex vivo* studies described earlier tracked the robots using clinical imaging systems such as fluoroscopy, ultrasound, and magnetic resonance imaging. Nevertheless, the resolution of current imaging modes is generally insufficient to distinguish the micro/nanorobots, particularly those at the nano-scale. For this reason, the configuration of robots in the swarm can help improve their visualization and monitoring *in vivo*. Therefore, in the design of future micro/nanorobots, it should be considered that they can be imaged with different imaging systems and can be changed according to the biological system used, size of animal model, and application.

Thus, the current challenge in micro/nano robotics lies in innovatively designing new robots for biofilm treatment and employing nanomaterials with diverse physical and chemical functionalities to eradicate bacteria. These robots should be capable of precise motion under specific actuation and amenable to imaging through various technologies.

Conflicts of interest

There are no conflicts to declare.

Acknowledgements

The work was supported by ERDF/ESF project TECHSCALE (no. CZ.02.01.01/00/22_008/0004587) and Research Fellow Scheme from the Hong Kong Research Grants Council (no. RFS2122-4S03). This research was co-funded by the European Union under the REFRESH-Research Excellence For REgion Sustainability and High-tech Industries project number CZ.10.03.01/00/22_003/0000048 *via* the Operational Programme Just Transition. L. Z. thanks the support from the SIAT-CUHK Joint Laboratory of Robotics and Intelligent Systems and the Multi-scale Medical Robotics Centre (MRC), InnoHK, at the Hong Kong Science Park. The TOC figure was generated using ChatGPT 4.0.

Notes and references

1 K. Yuan, J. Bujalance-Fernández, B. Jurado-Sánchez and A. Escarpa, *Microchim. Acta*, 2020, **187**, 581.
2 M. Fernández-Medina, M. A. Ramos-Docampo, O. Hovorka, V. Salgueiriño and B. Städle, *Adv. Funct. Mater.*, 2020, **30**, 1908283.
3 H. Zhou, C. C. Mayorga-Martinez, S. Pané, L. Zhang and M. Pumera, *Chem. Rev.*, 2021, **121**, 4999.
4 X.-Z. Chen, M. Hoop, F. Mushtaq, E. Siringil, C. Hu, B. J. Nelson and S. Pané, *Appl. Mater. Today*, 2017, **9**, 37.
5 J. Li, C. C. Mayorga-Martinez, C. D. Ohl and M. Pumera, *Adv. Funct. Mater.*, 2022, **32**, 2102265.
6 D. Jin, K. Yuan, X. Du, Q. Wang, S. Wang and L. Zhang, *Adv. Mater.*, 2021, **33**, 2100070.
7 B. Wang, K. Kostarelos, B. J. Nelson and L. Zhang, *Adv. Mater.*, 2021, **33**, 2002047.
8 Z. Zhang, L. Wang, T. K. F. Chan, Z. Chen, M. Ip, P. K. S. Chan, J. J. Y. Sung and L. Zhang, *Adv. Healthcare Mater.*, 2022, **11**, 2101991.
9 Y. Dong, L. Wang, V. Iacovacci, X. Wang, L. Zhang and B. J. Nelson, *Matter*, 2022, **5**, 77.
10 Y. Dong, C. Yi, S. Yang, J. Wang, P. Chen, X. Liu, W. Du, S. Wang and B.-F. Liu, *Nanoscale*, 2019, **11**, 4562.
11 F. Zhang, J. Zhuang, Z. Li, H. Gong, B. Esteban-Fernández de Ávila, Y. Duan, Q. Zhang, J. Zhou, L. Yin, E. Karshalev, W. Gao, V. Nizet, R. H. Fang, L. Zhang and J. Wang, *Nat. Mater.*, 2022, **21**, 1324.
12 F. Zhang, Z. Li, Y. Duan, A. Abbas, R. Mundaca-Uribe, L. Yin, H. Luan, W. Gao, R. H. Fang, L. Zhang and J. Wang, *Sci. Robot.*, 2022, **7**, eabo4160.
13 V. de la Asunción-Nadal, D. Rojas, B. Jurado-Sánchez and A. Escarpa, *J. Mater. Chem. A*, 2023, **11**, 1239.
14 R. Maria-Hormigos, B. Jurado-Sánchez and A. Escarpa, *Anal. Bioanal. Chem.*, 2022, **414**, 7035.
15 C. C. Mayorga-Martinez, M. Fojtů, J. Vyskočil, N.-J. Cho and M. Pumera, *Adv. Funct. Mater.*, 2022, **32**, 2207272.
16 E. Rahimi, R. Sanchis-Gual, X. Chen, A. Imani, Y. Gonzalez-Garcia, E. Asselin, A. Mol, L. Fedrizzi, S. Pané and M. Lekka, *Adv. Funct. Mater.*, 2023, 2210345.
17 H. Wang and M. Pumera, *Chem. Soc. Rev.*, 2020, **49**, 3211.

18 J. Wu, D. Folio, J. Zhu, B. Jang, X. Chen, J. Feng, P. Gambardella, J. Sort, J. Puigmartí-Luis, O. Ergeneman, A. Ferreira and S. Pané, *Adv. Intell. Syst.*, 2022, **4**, 2200192.
19 A. Terzopoulou, M. Palacios-Corella, C. Franco, S. Sevim, T. Dysli, F. Mushtaq, M. Romero-Angel, C. Martí-Gastaldo, D. Gong, J. Cai, X.-Z. Chen, M. Pumera, A. J. de Mello, B. J. Nelson, S. Pané and J. Puigmartí-Luis, *Adv. Funct. Mater.*, 2022, **32**, 2107421.
20 F. Ji, Y. Wu, M. Pumera and L. Zhang, *Adv. Mater.*, 2023, **35**, 2203959.
21 L. Yang and L. Zhang, *Annu. Rev. Control Robot. Auton. Syst.*, 2021, **4**, 509.
22 Q. Wang and L. Zhang, *IEEE Open J. Nanotechnol.*, 2020, **1**, 6.
23 L. Yang, J. Yu, S. Yang, B. Wang, B. J. Nelson and L. Zhang, *IEEE Trans. Robot.*, 2021, **38**, 1531.
24 H.-C. Flemming, T. R. Neu and D. L. J. Wozniak, *J. Bacteriol.*, 2007, **189**, 7945.
25 A. W. Decho, *Cont. Shelf Res.*, 2000, **20**, 1257.
26 L. Karygianni, Z. Ren, H. Koo and T. Thurnheer, *Trends Microbiol.*, 2020, **28**, 668.
27 L. K. Vestby, T. Grønseth, R. Simm and L. L. Nesse, *Antibiotics*, 2020, **9**, 59.
28 W. Zimmerli and C. Moser, *FEMS Microbiol. Immunol.*, 2012, **65**, 58.
29 T. Tolker-Nielsen, in *Biofilm Development, Microbial Biofilms*, ed. M. Ghannoum, M. Parsek, M. Whiteley and P. K. Mukherjee, 2015.
30 G. Lambert, A. Bergman, Q. Zhang Bortz and R. Austin, *New J. Phys.*, 2014, **16**, 045005.
31 T. Karaguler, H. Kahraman and M. Tuter, *Biocybern. Biomed. Eng.*, 2017, **37**, 336.
32 K. Sauer, P. Stoodley, D. M. Goeres, L. Hall-Stoodley, M. Burmølle, P. S. Stewart and T. Bjarnsholt, *Nat. Rev. Microbiol.*, 2022, **20**, 608.
33 Q. Chi, Z. Wang, F. Tian, J. You and S. Xu, *Micromachines*, 2018, **9**, 537.
34 M. Guix, C. C. Mayorga-Martinez and A. Merkoçi, *Chem. Rev.*, 2014, **114**, 6285.
35 K. Villa, J. Viktorova, J. Plutnar, T. Ruml, L. Hoang and M. Pumera, *Cell Rep. Phys. Sci.*, 2020, **1**, 100181.
36 H. Ji, H. Hu, Q. Tang, X. Kang, X. Liu, L. Zhao, R. Jing, M. Wu, G. Li, X. Zhou, J. Liu, Q. Wang, H. Cong, L. Wu and Y. Qin, *J. Hazard. Mater.*, 2022, **436**, 129210.
37 Y.-H. Deng, T. Ricciardulli, J. Won, M. A. Wade, S. A. Rogers, S. A. Boppart, D. W. Flaherty and H. Kong, *Biomaterials*, 2022, **287**, 121610.
38 V. Milosavljevic, L. Kosaristanova, K. Dolezelikova, V. Adam and M. Pumera, *Adv. Funct. Mater.*, 2022, **32**, 2112935.
39 K. Villa, H. Sopha, J. Zelenka, M. Motola, L. Dekanovsky, D. C. Beketova, J. M. Macak, T. Ruml and M. Pumera, *Small*, 2022, **18**, 2106612.
40 K. Yuan, B. Jurado-Sanchez and A. Escarpa, *Angew. Chem., Int. Ed.*, 2021, **60**, 4915.
41 M. M. Stanton, B.-W. Park, D. Vilela, K. Bente, D. Faivre, M. Sitti and S. Sanchez, *ACS Nano*, 2017, **11**, 9968.
42 C. C. Mayorga-Martinez, J. Zelenka, J. Grmela, H. Michalkova, T. Ruml, J. Mareš and M. Pumera, *Adv. Sci.*, 2021, **8**, 2101301.
43 V. Magdanz, I. S. M. Khalil, J. Simmchen, G. P. Furtado, S. Mohanty, J. Gebauer, H. Xu, A. Klingner, A. Aziz, M. Medina-Sánchez, O. G. Schmidt and S. Misra, *Sci. Adv.*, 2020, **6**, eaba5855.
44 L. Kong, C. C. Mayorga-Martinez, J. Guan and M. Pumera, *Small*, 2020, **16**, 1903179.
45 A.-I. Bunea, D. Martella, S. Nocentini, C. Parmeggiani, R. Taboryski and D. S. Wiersma, *Adv. Intell. Syst.*, 2021, **3**, 2000256.
46 W. Yang, X. Wang, Z. Wang, W. Liang and Z. Ge, *Opt. Lasers Eng.*, 2023, **161**, 107380.
47 W. Wang, G. Huang, J. C. Yu and P. K. Wong, *J. Environ. Sci.*, 2015, **34**, 232.
48 J. He, A. Kumar, M. Khan and I. M. C. Lo, *Sci. Total Environ.*, 2021, **758**, 143953.
49 T. Cui, S. Wu, Y. Sun, J. G. Ren and X. Qu, *Nano Lett.*, 2020, **20**, 7350.
50 M. Ussia, M. Urso, K. Dolezelikova, H. Michalkova, V. Adam and M. Pumera, *Adv. Funct. Mater.*, 2021, **31**, 2101178.
51 M. Ussia, M. Urso, S. Kment, T. Fialova, K. Klima, K. Dolezelikova and M. Pumera, *Small*, 2022, **18**, 2200708.
52 D. Rojas, M. Kuthanova, K. Dolezelikova and M. Pumera, *NPG Asia Mater.*, 2022, **14**, 63.
53 G. Gardi, S. Ceron, W. Wang, K. Petersen and M. Sitti, *Nat. Commun.*, 2022, **13**, 2239.
54 G. Hwang, A. J. Paula, E. E. Hunter, Y. Liu, A. Babeer, B. Karabucak, K. Stebe, V. Kumar, E. Steager and H. Koo, *Sci. Robot.*, 2019, **4**, eaaw2388.
55 Y. Dong, L. Wang, K. Yuan, F. Ji, J. Gao, Z. Zhang, X. Du, Y. Tian, Q. Wang and L. Zhang, *ACS Nano*, 2021, **15**, 5056–5067.
56 C. C. Mayorga-Martinez, J. Zelenka, K. Klima, P. Mayorga-Burrezo, L. Hoang, T. Ruml and M. Pumera, *ACS Nano*, 2022, **16**, 8694.
57 M. Sun, K. F. Chan, Z. Zhang, L. Wang, Q. Wang, S. Yang, S. M. Chan, P. W. Y. Chiu, J. J. Y. Sung and L. Zhang, *Adv. Mater.*, 2022, **34**, 2201888.
58 C. C. Mayorga-Martinez, J. Zelenka, K. Klima, M. Kubanova, T. Ruml and M. Pumera, *Adv. Mater.*, 2023, 2300191.
59 Y. Dong, L. Wang, Z. Zhang, F. Ji, T. K. F. Chan, H. Yang, C. P. L. Chan, Z. Yang, Z. Chen, W. T. Chang, J. Y. K. Chan, J. J. Y. Sung and L. Zhang, *Sci. Adv.*, 2022, **8**, eabq8573.
60 M. Sitti and D. S. Wiersma, *Adv. Mater.*, 2020, **32**, 1906766.
61 W. Xiu, L. Ren, H. Xiao, Y. Zhang, D. Wang, K. Yang, S. Wang, L. Yuwen, X. Li, H. Dong, Q. Li, Y. Mou, Y. Zhang, Z. Yin, B. Liang, Y. Gao and L. Wang, *Sci. Adv.*, 2023, **9**, eade5446.
62 J. Wang, L. Wang, J. Pan, J. Zhao, J. Tang, D. Jiang, P. Hu, W. Jia and J. Shi, *Adv. Sci.*, 2021, **8**, 2004010.
63 G. Pietrocola, D. Campoccia, C. Motta, L. Montanaro, C. R. Arciola and P. Speziale, *Int. J. Mol. Sci.*, 2022, **23**, 5958.

64 G. Charles and M. S. Roberts, *Am. J. Infect. Control*, 2013, **41**, S77.
65 Y. Zheng, L. He, T. K. Asiamah and M. Otto, *Environ. Microbiol.*, 2018, **20**, 3141.
66 S. Bose and A. K. Ghosh, *J. Clin. Diagn. Res.*, 2011, **5**, 127.
67 M. Saini, Y. Singh, P. Arora, V. Arora and K. Jain, *World J. Clin. Cases*, 2015, **3**, 52.
68 M. Panchal, S. Khare, P. Khamkar and K. S. Bhole, *Mater. Today: Proc.*, 2022, **68**, 1860.
69 R. O. Darouiche, *N. Engl. J. Med.*, 2004, **350**, 1422.
70 A. D. Pye, D. E. A. Lockhart, M. P. Dawson, C. A. Murray and A. J. Smith, *J. Hosp. Infect.*, 2009, **72**, 104.
71 C. Scully, S. Sonis and P. D. Diz, *Oral Dis.*, 2006, **12**, 229.
72 L. J. A. Heitz-Mayfield and G. E. Salvi, *J. Clin. Periodontol.*, 2018, **45**, S237.
73 R. Pontoriero, M. P. Tonelli, G. Carnevale, A. Mombelli, S. R. Nyman and N. P. Lang, *Clin. Oral. Implants Res.*, 1994, **5**, 254.
74 W. H. Bowen, R. A. Burne, H. Wu and H. Koo, *Trends Microbiol.*, 2017, **26**, 229.
75 D. Asker, T. S. Awad, D. Raju, H. Sanchez, I. Lacdao, S. Gilbert, P. Sivarajah, D. R. Andes, D. C. Sheppard, P. L. Howell and B. D. Hatton, *ACS Appl. Bio Mater.*, 2021, **4**, 8248.
76 B. W. Trautner and R. O. Darouiche, *Am. J. Infect. Control*, 2004, **32**, 177.
77 D. Stickler, *Nat. Rev. Urol.*, 2008, **5**, 598.
78 Yang Wu, *et al.*, Gastric acid powered nanomotors release antibiotics for *in vivo* treatment of *Helicobacter pylori* infection, *Small*, 2021, **17**, 2006877.
79 L. Xie, X. Pang, X. Yan, Q. Dai, H. Lin, J. Ye, Y. Chen, Q. Zhao, X. Ma, X. Zhang, G. Liu and X. Chen, *ACS Nano*, 2020, **14**, 2880.
80 X. Arqué, M. D. T. Torres, T. Patiño, A. Boaro, S. Sánchez and C. de la Fuente-Nunez, *ACS Nano*, 2022, **16**, 7547.
81 M. J. Oh, A. Babeer, Y. Liu, Z. Ren, J. Wu, D. A. Issadore, K. J. Stebe, D. Lee, E. Steager and H. Koo, *ACS Nano*, 2022, **16**, 11998.
82 A. Babeer, M. J. Oh, Z. Ren, Y. Liu, F. Marques, A. Poly, B. Karabucak, E. Steager and H. Koo, *J. Dent. Res.*, 2022, **101**, 1009.